Biomech Model Mechanobiol (2011) 10:767–778
DOI 10.1007/s10237-010-0272-0

ORIGINAL PAPER

Estimating material parameters of a structurally based constitutive relation for skin mechanics

Jessica W. Y. Jor · Martyn P. Nash · Poul M. F. Nielsen · Peter J. Hunter

Received: 1 September 2010 / Accepted: 10 November 2010 / Published online: 25 November 2010

Abstract This paper presents a structurally based modeling framework to characterize the structure–function relation in skin tissues, based upon biaxial tensile experiments performed in vitro on porcine skin. Equi-axial deformations were imposed by stretching circular skin specimens uniformly along twelve directions, and the resultant loads at the membrane attachment points were measured. Displacement fields at each deformation step were tracked using an image 2D cross-correlation technique. A modeling framework was developed to simulate the experiments, whereby measured forces were applied to finite element models that were created to represent the geometry and structure of the tissue samples. Parameters of a structurally based constitutive relation were then identified using nonlinear optimization. Results showed that the ground matrix stiffness ranged from 5 to 32 kPa, fiber orientation mean from 2 to 13° from the torso midline, fiber undulation mean from 1.04 to 1.34 and collagen fiber stiffness from 48 to 366 MPa. It was concluded that the objective function was highly sensitive to the mean orientation and that a priori information about fiber orientation mean was important for the reliable identification of constitutive parameters.

Keywords Skin · Biomechanics · Collagen · Material parameter identification · Porcine

J. W. Y. Jor (✉) · M. P. Nash · P. M. F. Nielsen · P. J. Hunter
Auckland Bioengineering Institute, University of Auckland,
70 Symonds Street, Auckland, New Zealand
e-mail: j.jor@auckland.ac.nz

M. P. Nash · P. M. F. Nielsen
Department of Engineering Science, University of Auckland,
70 Symonds Street, Auckland, New Zealand

1 Introduction

Human skin displays nonlinear, heterogeneous, anisotropic and viscoelastic mechanical properties, which are strongly influenced by the architecture and mechanical response of its microstructural components (Wilkes et al. 1973). Craik and McNeil (1965) were among the first researchers to histologically show the alignment of collagen fibers under mechanical loading of abdominal human skin. Subsequently, similar observations were made from images obtained using scanning electron microscopy (SEM) by Finlay (1969). The typical stress–strain response of skin subjected to mechanical stress has been well established (Daly 1966). There are three main phases, as shown in Fig. 1. The initial phase, or the low dynamic stiffness region, corresponds to a gradual increase in stress with strain. This is thought to be due to the reorientation of fibers toward the axis of loading, followed by their straightening. Since the majority of fibers are initially undulated, the load required to reorient and straighten them is small. The second phase represents gradual stiffening when an increasing number of fibers become progressively aligned and load bearing when fibers are stretched. Due to variation in the extent of fiber undulations, fibers begin to resist tension at different stages, and this is reflected by the nonlinear mechanical response of skin. The final phase is an almost linear region showing greater stress at higher strains. Since the majority of fibers are aligned and stretching at this stage, the overall mechanical response becomes dependent upon the intrinsic mechanical properties of the fibers themselves. Deformation beyond the final phase leads to yielding and rupture of the skin (Wilkes et al. 1973). The geometrical arrangement of fibers plays a critical role in determining the mechanical response of skin. The observed anisotropic behavior is, in part, due to the varying degrees of packing of interweaving fibers throughout the depth of

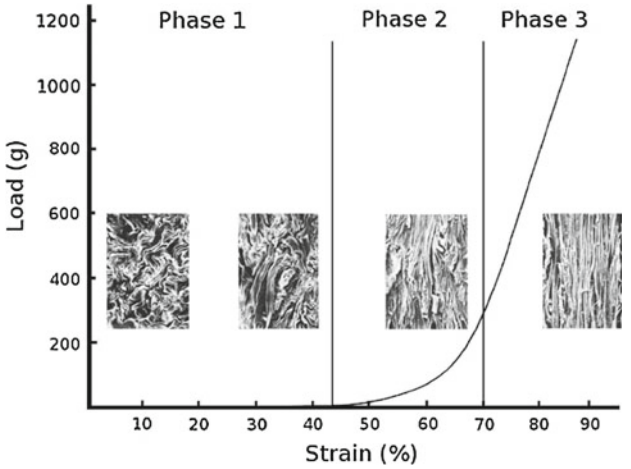

Fig. 1 Load–strain response of an in vitro uniaxial tensile test of human abdominal skin and corresponding organization of collagen fibers in parallel sections of the dermis. Collagen fibers are undulated in a multi-directional system at the beginning of Phase 1, before becoming aligned along the load axis at the end of Phase 1. At the end of Phase 2, fibers are aligned and almost straight. During Phase 3, fibers are aligned and straight. Reproduced from Brown (1973)

the dermis. Experiments in which elastin and ground substance were digested showed that elastin contributes to the mechanical response of skin only at low tissue strains, while the contribution from ground substance is small (Daly 1969; Harkness and Harkness 1959).

Researchers have attempted to model the mechanical response of connective tissues by taking one of two main approaches: a phenomenological approach in which mathematical expressions are chosen to best fit experimental data or reflect material behavior; or a structural approach in which constitutive relations are based on the structural arrangement of the constituents. Phenomenological models cover a broad range of mathematical functional forms, with the power and exponential forms considered as most common to model elastic stress–strain behavior of connective tissues (Fung 1967; Tong and Fung 1976). One disadvantage of phenomenological models is that, despite being able to accurately represent tissue behavior, predictability remains a troublesome issue and the parameters obtained for phenomenological models cannot be directly related to specific biological features of skin (Rodrigues 2001). In contrast, structural models derive constitutive relations based in part upon the underlying histology. Thus, the structural approach to mathematical models is capable of providing important insights into the structure–function relationship of a specific tissue. Perhaps one of the most extensive approaches to structurally based constitutive relations of collagenous tissues was presented by Lanir (1979, 1983), who was one of the first to formulate a constitutive relation taking into consideration the geometric arrangements of fiber networks in soft biological tissues. Structurally based constitutive relations have been developed for a variety of tissues such as tendon/ligament (Hurschler et al. 1997), arterial walls (Holzapfel et al. 2002), pericardium (Sacks 2003), passive myocardium (Horowitz et al. 1988; Holzapfel and Ogden 2009) and heart valves (Billiar and Sacks 2000).

Although a large number of experiments have been conducted over the years on measuring the structural and functional properties of skin, standardization of such measurements and interpretation of results are difficult to establish. Data obtained are often expressed as indices, primarily stretchability or stretchability ratios, which are highly dependent upon the experimental conditions (Diridollou et al. 2000). Challenges in standardizing such definitions and interpretation have been described by Barel et al. (1995). In many cases, the complex structure of skin has been simplified to a homogeneous nonlinear elastic solid and represented by a simple constitutive relation. Often the different regions of the typical J-curve stress–strain plot are modeled separately using a neo-Hookean description and a Young's modulus, calculated for one particular region, without a clear description of which part of the nonlinear curve it was derived from. Biaxial tensile tests have been previously performed to measure the mechanical response of skin (Lanir and Fung 1974; Reihsner et al. 1995; Kvistedal and Nielsen 2009), but few attempts have been made to represent observed behavior with appropriate constitutive relations (Meijer et al. 1999; Lokshin and Lanir 2009).

Identification of model parameters of structurally based constitutive relations may be greatly simplified since structural parameters can be estimated directly from imaging. In order to be able to understand and quantify the relationship between microstructure and the mechanical function of skin, specific quantitative data on collagen fiber orientation is required. In our laboratory, the dermal collagen network in transverse sections of porcine skin has been studied using confocal laser scanning microscopy (CLSM) (Jor et al. 2010). Thick collagen bundles were observed to cross obliquely in two main directions, between the epidermis and hypodermis (Fig. 2). A similar fiber lattice arrangement was observed in transverse planes sectioned at different orientations with respect to the torso midline, such that that the collagen fibers form an interwoven network that exhibits common structure about the normal direction to the epidermis. Fiber orientations were extracted using a structure tensor algorithm. It has been demonstrated that the distribution of fiber orientations may be quantified, and represented, by a two-parameter probability density distribution.

Since the structure of skin is highly correlated to its function, the development of a structurally based biomechanical model is useful to help understand the underlying function of not only healthy skin, but also damaged or diseased skin. This is highlighted by the fact that changes to the structural arrangement of collagen are often associated with

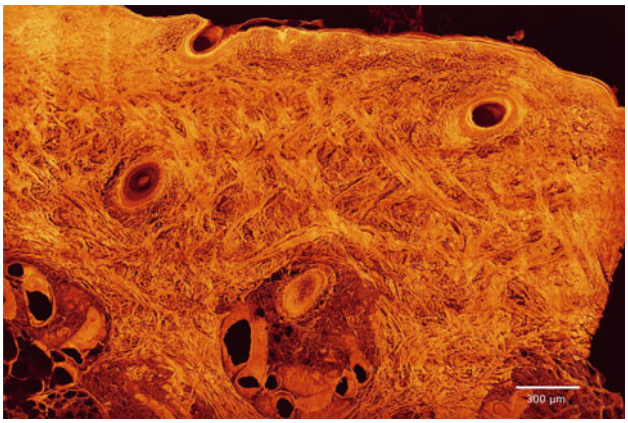

Fig. 2 A 60 µm saggital section of porcine skin imaged using confocal laser scanning microscopy (CLSM), with picrosirius red stained collagen appearing bright. Collagen fibers form a distinct lattice arrangement, with fibers aligned along two predominant directions that run obliquely from the upper to lower reticular dermis (Jor et al. 2010)

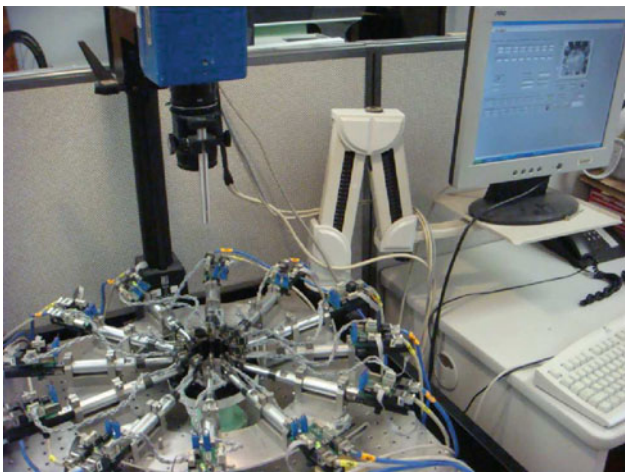

Fig. 3 The multiaxial tensile rig consists of a circular array of 12 automated motor axes with displacement actuators and force transducers attached, a CCD camera mounted above the testing region and the computer system required to control the device

pathological disorders, such as the Ehlers–Danlos syndrome which is a connective tissue disorder caused by a defect in the synthesis of collagen (Pope et al. 1975). A structurally based biomechanical model of the skin would allow one to investigate the effects of individual dermal components on the overall macroscopic tissue response.

2 Materials and methods

2.1 Multiaxial tensile experiments

To investigate the mechanical properties of skin, in vitro tensile tests were performed on porcine skin using a custom-built multiaxial tensile rig (Nielsen et al. 2002). The rig consisted of twelve *Physik Instrumente* DC-Mike M-226 actuators arranged in a circular array with 30° spacing (Fig. 3). Each actuator had a displacement range of 50 mm and resolution of 0.2 µm. Custom-built 2D force transducers were mounted on the tips of the displacement actuators to record the corresponding force vector measured perpendicular to each of the twelve attachment pins. Each force transducer was constructed of two pairs of strain gauges bonded in a half-bridge configuration to the four necked surfaces of a cantilever. Each pair of opposite faces was responsible for measuring the x and y components of the force vector. Images of the specimen geometry were captured using a *Atmel* Camelia 4M CCD camera with 2,048 pixel × 2,048 pixel, which was mounted overlooking the surface of the specimen. In order to estimate the deformed geometry at each loading step, a speckle pattern was created on the surface of the specimen, using a *Harder and Steenbeck* Infinity airbrush, to enable tracking of material points. A phase corrected cross-correlation technique (Malcolm 2000) was used to compute the displacements of 64 pixel × 64 pixel subimages and thus material points between successive deformation steps. The cross-correlation technique is capable of resolving displacements as small as 0.008 of a pixel, corresponding to a resolution for the measured displacements of ∼0.3 µm.

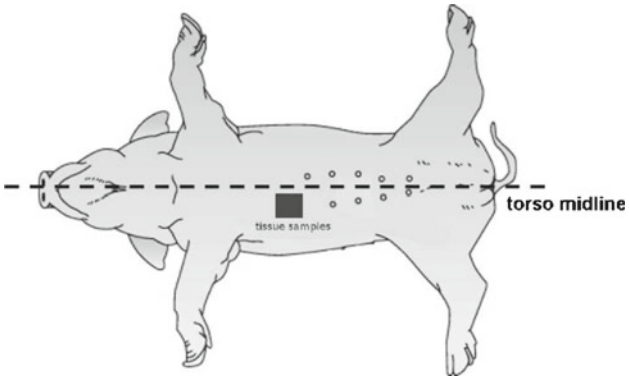

Fig. 4 Schematic diagram showing the location of excised samples in relation to the animal's torso midline

Three skin samples (labeled 7C5, 9B4, 9C5) were obtained from two young pigs within 1 h of the animals being sacrificed for other medical research purposes. The surface of the test area was shaved and cleaned with *DO Weaver* NuPrep to allow clear marking on the skin. A custom template was used to determine the positions of the twelve attachment points arranged in a circle (∅60 mm) within each sample while the tissue was still intact. Square samples 70 mm × 70 mm were excised from the abdominal region of each pig along the medial midline (Fig. 4), and they were stored in phosphate-buffered solution (PBS) at room temperature (∼ 21°C) before testing. Mechanical tests were conducted within 12 h post-tissue excision. Prior to the experiments, the fat layer

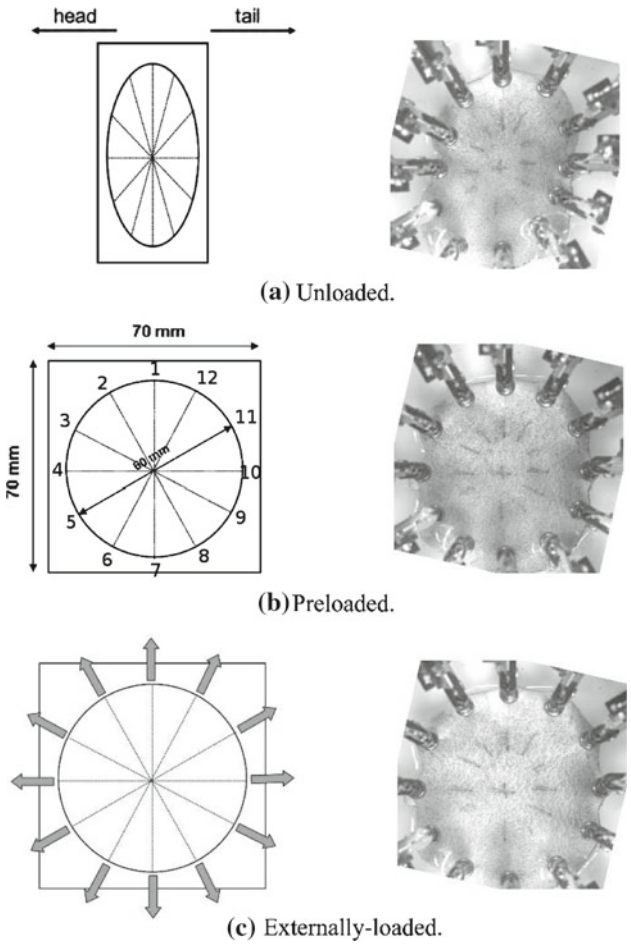

Fig. 5 Three configurations of a tissue sample: unloaded (**a**), preloaded (**b**) and externally loaded (**c**). The schematic diagrams are shown on the *left* acquired images of sample 7C5 are shown on the *right*

was removed as much as possible (without damaging the skin layers) so that the mechanical contribution due to the hypodermis could be minimized.

For the tissue samples used in this study, three different geometric configurations (Fig. 5) were considered and the following terms are used to describe them:

1. *Unloaded:* the geometry of the sample after it was excised from the animal and allowed to retract on a frictionless surface (i.e., free from pretension and applied loads);
2. *Preloaded:* the state when the tissue was subjected to the effects of pretension to mimic its state when intact in the animal (in vivo);
3. *Externally loaded:* the state when external loads were applied to a preloaded sample.

The unloaded geometry was required to determine the pretension for each sample. This was obtained by allowing the sample to relax in PBS over a period of 3–4 h. An image of the unloaded specimen, floating in PBS to remove any effects of surface friction, was captured with the CCD camera. Changes in length along each of the six axes of the load cells were estimated by digitizing the positions of each attachment point in the image. A speckle pattern was applied to the surface of the sample before it was attached to the rig in its unloaded configuration. Displacements were applied over a total of 30 increments to stretch the specimen from its unloaded to preloaded configurations; an image was captured at each step to enable tracking of material points. The measured forces required to transform the specimen from its unloaded to preloaded states were referred to as the *pretension* forces.

From the preloaded state, equi-axial deformations were imposed by stretching the specimen uniformly along each of the 12 directions. A stress relaxation interval of 30 s (Kvistedal and Nielsen 2009) was allowed after each displacement increment before any boundary forces and the geometry of the sample were recorded. The specimen was stretched incrementally until any one transducer became saturated at 1 N, resulting in the maximum displacement ranging from 2.7 to 3.2 mm of stretch along each of the axes from the preloaded configuration. Once the maximum displacement achievable for each specimen was determined from the first load cycle, subsequent cycles were repeated by applying 10 equal position increments up to the maximum displacement. Equibiaxial loading was repeated at least five times for each specimen. To obtain an unloading stress–strain curve, the sequence of loading positions were reversed. To minimize the accumulation of any measurement errors between cycles, all forces and deformations were recorded as perturbations from the preloaded configuration within each loading and unloading cycle. In order to maintain hydration of the specimen during mechanical testing, the specimen was immersed in a PBS bath throughout the experiment.

2.2 Modeling framework

2.2.1 Constitutive relation

A structurally based constitutive relation was used to describe the mechanical behavior of skin tissues, taking into consideration the geometric arrangement of the collagen network (Lanir 1983). In this microstructural model, a network of collagen fibers with varying orientations was embedded in a tissue block of ground matrix. The tissue block was assumed to be very small compared to the whole tissue, such that the material can be assumed to be homogeneous within each block and that the deformation field varies linearly over the block. The following model assumptions were made:

– Each fiber is undulated and only resists load when completely straightened.

- Fibers can only resist tensile loading and buckle under compressive loads, i.e., no load is required to fold or unfold fibers.
- Each fiber undergoes a uniaxial strain, which is the tensorial transformation of the macroscopic tissue strain along the fiber direction (affine deformation). The justification for this assumption is provided by the abundance of interconnections (attachments) between the different fibers.
- The fibers are linearly elastic when stretched and their mechanical properties are governed by a 1D fiber load–stretch relation.
- The ground matrix behaves like an isotropic neo-Hookean material.
- The material properites are assumed to be homogeneous across each of the tissue samples.
- Viscoelastic effects are neglected.

The full details of the development of this model are contained within Lanir (1983), but a brief summary of the relevant equations are contained here for completeness.

The second Piola–Kirchhoff stress tensor, $\mathbf{S}$, sums the contributions from the ground matrix $\mathbf{S}^m$ and collagen fibers $\mathbf{S}^f$, respectively, by taking into consideration the fiber volume fraction V_f, such that

$$\mathbf{S} = (1 - V_f) \cdot \mathbf{S}^m + V_f \cdot \mathbf{S}^f \tag{1}$$

The ground matrix was assumed to be a neo-Hookean material; thus, the strain energy function of the ground matrix (W_m) is given by

$$W_m = K_m(I_1 - 3) \tag{2}$$

where K_m is the stiffness of the ground matrix and I_1 is the first principal strain invariant. For a 2D membrane, the 2nd Piola–Kirchhoff stress tensor for the ground matrix can be expressed as

$$S_{ij}^m = \frac{\partial W_m}{\partial E_{ij}} = \frac{\partial W_m}{\partial I_1}\frac{\partial I_1}{\partial E_{ij}} = \begin{cases} 2K_m & i = j \\ 0 & i \neq j \end{cases} \tag{3}$$

where $\mathbf{E}$ is the Green–Langrage strain tensor. A uniaxial fiber strain energy function (w_f) is defined as a function of the fiber stretch ratio λ

$$w_f = \frac{K_c}{2}(\lambda - 1)^2 \tag{4}$$

where K_c is the collagen fiber stiffness and λ is given by Eq. 5.

$$\begin{aligned} \lambda &= \sqrt{2\gamma_f' + 1} \\ &= \sqrt{2(E_{11}\cos^2\theta + E_{22}\sin^2\theta + 2E_{12}\cos\theta\sin\theta) + 1} \end{aligned} \tag{5}$$

where γ_f' represents the strain along the fiber in the deformed configuration and θ is the in-plane fiber angle.

The load per unit undeformed cross-sectional area in the fiber is

$$f(\lambda) = \frac{\partial w_f(\lambda)}{\partial \lambda} = \begin{cases} K_c(\lambda - 1) & \lambda > 1 \\ 0 & \lambda \leq 1 \end{cases} \tag{6}$$

The total strain energy of all fibers in an undeformed volume unit, W_f, is given by

$$W_f = \sum_{\theta} \cdot R(\theta) \cdot w_f(\lambda) \cdot \Delta\theta \tag{7}$$

where R is the probability density function for the fiber orientation. The summation can be replaced by integrals if there is a large enough number of fibers in each direction.

For a 2D membrane, the 2nd Piola–Kirchhoff stress tensor for the fibers can be expressed as

$$S_{ij}^f = \int_{\theta} R(\theta)\frac{1}{\lambda}\frac{\partial \gamma_f'}{\partial E_{ij}} \cdot \int_{x=1}^{\lambda} D(x) \cdot f\left(\frac{\lambda}{x}\right) \mathrm{d}x\mathrm{d}\theta \tag{8}$$

where x is the stretch required to straighten an undulated fiber and $D(x)$ is the probability density function for fiber undulation.

A unimodal π-periodic von Mises distribution was chosen to describe the in-plane fiber orientation, θ (Eq. 9).

$$R(\theta) = \frac{\exp\left[\kappa_\theta \cos(2(\theta - \mu_\theta))\right]}{\pi I_0(\kappa_\theta)} \tag{9}$$

where μ_θ is the fiber orientation mean, κ is the spread and $I_0(\kappa)$ is the modified Bessel function of order zero (Eq. 10).

$$I_0(\kappa) = \frac{1}{\pi}\int_0^{\pi} \exp[\kappa\cos 2\theta]\mathrm{d}\theta \tag{10}$$

Eq. 9 must also satisfy the following normalization constraint

$$\int_{\theta=-\frac{\pi}{2}}^{\theta=+\frac{\pi}{2}} R(\theta)\mathrm{d}\theta = 1 \tag{11}$$

The distribution function for fiber undulation is assumed to be Gaussian and can thus be defined by:

$$D(x) = \frac{1}{\sqrt{2\pi}\sigma_x}\exp\left\{-\frac{(x - \mu_x)^2}{2\sigma_x^2}\right\} \tag{12}$$

where μ_x and σ_x are the mean and standard deviation (SD) of the undulation distribution, respectively.

2.2.2 Finite element models

In order to interpret measurements of displacement field data in a quantitatively meaningful manner, a mathematical modeling framework was developed to simulate the mechanical

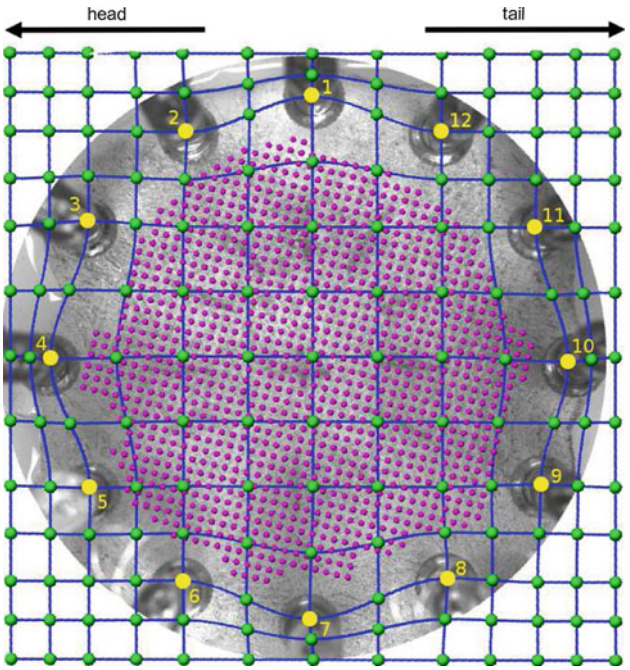

Fig. 6 Finite element (FE) mesh (*green dots and blue lines*) of a sample in its preloaded configuration. The image of the sample captured during mechanical experiments is shown as the background. The 12 attachment nodes are shown as *yellow dots*; the grid of material points at the preloaded configuration are shown as *pink dots*. The FE mesh with respect to the animal's body coordinates is shown

experiments using finite element (FE) modeling. FE models were created, using in-house software CMISS[1] to represent the preloaded geometries of skin tissue samples used for mechanical testing. They consisted of 2D square meshes with 12 of the 169 nodes positioned at specific positions to form a circular array (Fig. 6). These nodes served as attachment points of the tissue to the multiaxial rig and will be referred to as *attachment nodes*. In order to generate accurate and specific meshes for each tissue sample, the attachment nodes were digitized from an image of the mounted sample in the multiaxial rig in its preloaded configuration. Bicubic Hermite quadrilateral elements (Bradley et al. 1997) were used for all meshes in this study. A grid of approximately 1,200 material points was embedded within each mesh, and the displacements of these points were mathematically tracked between successive loading steps. Forces measured during the tensile experiments were applied at the 12 attachment nodes as boundary constraints. Comparison was made between experimentally tracked and model-predicted displacements of the material points.

2.3 Material parameter identification

The preloaded configuration of the tissue samples was treated as the reference geometry for parameter estimation. A set of initial parameter values were used in a forward mechanics solution process, whereby experimental forces were applied at the 12 attachment nodes as boundary constraints. The nonlinear *lsqnonlin* optimization function in Matlab[2], which is based upon *trust regions*, was used to minimize the following objective function in a least-squares sense

$$\Omega(\vartheta) = \sum_{i=1}^{n} (\mathbf{y}_i^{\text{expt}} - \mathbf{y}_i^{\text{model}}(\vartheta))^2 \tag{13}$$

where n is the number of material points (about 1,200 in this study), ϑ is the current set of material parameters, $\mathbf{y}_i^{\text{expt}}$ is the positions of the experimentally tracked material points and $\mathbf{y}_i^{\text{model}}(\vartheta)$ is the model-predicted positions of the material points. An optimal solution was obtained when the change in material parameters was less than 10^{-5} mm^2, or the change in the objective function was less than 10^{-9} mm^2.

Due to the large number of parameters in the constitutive relation described in Sect. 2.2.1, which appeared to have "trade-off" effects against each other, the number of estimated parameters was limited to subsets. In the identification procedure, two different estimation strategies were investigated, as listed in Table 1. The parameters to be identified for *Strategy A* were fiber orientation mean (μ_θ), collagen fiber stiffness (K_c) and ground matrix stiffness (K_m); for *Strategy B*, parameters were the fiber orientation mean (μ_θ), fiber undulation mean (μ_x) and ground matrix stiffness (K_m). The fixed parameters for both strategies were fiber orientation spread (κ), fiber undulation SD (σ_x) and fiber volume fraction (V_f). σ_x and V_f were fixed to 0.2 and 1.2, respectively, with both values previously reported in the literature (Table 2). κ was fixed to 10 (equivalent to a circular SD of 21°) based upon quantitative analysis of collagen orientation in porcine skin (Jor et al. 2010). All parameters included in the optimization procedure were subjected to physiological lower and upper bounds. In order to investigate the identifiability of the parameters, both estimation strategies were performed starting from 10 different sets of initial estimates (random numbers generated between the lower and upper bounds of each parameter).

Three measures of optimality criteria for parameter identification were used, as proposed by Nathanson and Saidel (1985), are described below:

1. *D-optimality* The D-optimality attempts to minimize the volume of the ϵ-indifference region, resulting in least variance in all parameters. Since the ϵ-indifference region is inversely proportional to the determinant of the Hessian at the optimum, det($\mathbf{H}_0$), the goal is then to maximize det($\mathbf{H}_0$). This is widely regarded as the most important criterion in parameter estimation.

[1] www.cmiss.org.

[2] www.mathworks.com.

Table 1 List of parameters for a 2D a structural constitutive relation with the corresponding lower/upper bounds and values from the literature (see Table 2)

Type	Parameter	Description	L.B.	U.B.	Strategy A	Strategy B
Structural	Fiber orientation θ	Mean μ_θ	0	π	Free	Free
		Spread κ_θ	–	–	Fixed at 10	Fixed at 10
	Fiber undulation x	Mean μ_x	1.0	1.8	Fixed at 1.2	Free
		SD σ_θ	–	–	Fixed at 0.2	Fixed at 0.2
	Fiber volume fraction V_f		–	–	Fixed at 0.3	Fixed at 0.3
Nonstructural	Collagen fiber stiffness	K_c	0.3 MPa	500 MPa	Free	Fixed at 100 MPa
	Ground matrix stiffness	K_m	1 kPa	100 kPa	Free	Free

Table 2 Values of material parameters that have been previously reported

Parameter	Description	Reported values
μ_x	Fiber undulation mean	1.2–1.6 (Manschot 1985)
σ_x	Fiber undulation SD	0.2 (Manschot 1985)
K_c	Collagen fiber stiffness	100 MPa (Viidik 1980)
V_f	Fiber volume fraction	0.3 (Manschot 1985)

2. *Condition number of the Hessian* The condition number of $\mathbf{H}_0$ is defined as the ratio between the smallest and largest eigenvalues of $\mathbf{H}_0$. When the value of cond($\mathbf{H}_0$) is close to 1, the axes of the hyperellipsoid approach equal lengths, reflecting low anisotropy (or eccentricity) in the neighborhood of the optimum. An important thing to note is that this criterion does not indicate the volume change of the hyperellipsoid; thus, it should only be included as a secondary optimality criterion.
3. *M-optimality* The above-mentioned criteria do not take into account the degree of interaction between parameters, which is associated with the orientation of the indifference region with the material parameter axes. The goal is to minimize the off-diagonal terms of $\mathbf{H}_0$, or the angle between the orientation of the indifference region and the material parameter axes. To determine the M-optimality, a scaled Hessian ($\tilde{\mathbf{H}}$) must first be computed, whose components are defined as

$$\tilde{h}_{ij} = \frac{h_{ij}}{\sqrt{h_{ii}h_{jj}}} \qquad i, j \text{ not summed} \tag{14}$$

The M-optimality criterion aims to maximize det($\tilde{\mathbf{H}}$) toward the value of 1. This indicates no interaction between the parameters since the hyperellipsoid and material parameter axes are completely aligned. It has been shown $0 < \det(\tilde{\mathbf{H}}) \leq 1$.

Table 3 Dimensions of tissue samples in their unloaded configuration for each sample

Dimension (mm)	7C5	9B4	9C5
Unloaded width	41.1	43.8	42.3
Unloaded length	55.8	53.7	57.1

3 Results

3.1 Pretension measurements

From images of the unloaded tissue samples, the originally square-shaped specimens (70 mm × 70 mm) deformed to rectangular-shaped specimens such that most retraction occurred in the direction parallel to the torso midline. This observation is consistent with the previously reported direction of Langer's lines for pigs, which run parallel to the torso midline (Rose et al. 1976). The dimensions of the tissue samples following tissue relaxation are given in Table 3. The averaged width and length measurements were calculated from two measurements at the outer boundaries and one measurement at the center of the specimen. In general, the tissue samples retracted ∼ 40% in width and ∼ 20% in length from the preloaded (in vivo) to the unloaded configuration.

The pretension forces were recorded for each of the 12 directions (Fig. 7). The greatest pretension was measured in directions coinciding with greatest retraction. Pretension forces were much smaller than the forces measured when an external load was applied. The average measured pretension was as low as ∼ 2% of the average measured external forces at approximately 12% stretch.

3.2 Optimal solutions

The optimal solutions for all tissue samples, using *Strategy A* (the optimized parameters were K_m, μ_θ and K_c), are given

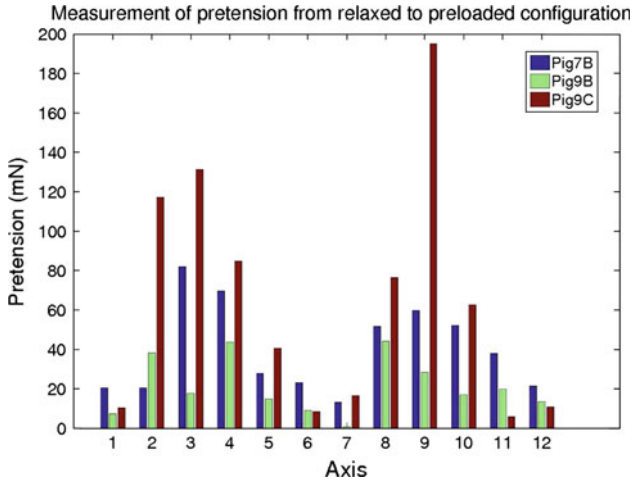

Fig. 7 Bar graph of pretension forces measured for each tissue specimen along the 12 motor axes. The *Langer's lines* coincide with axis 4 and axis 10

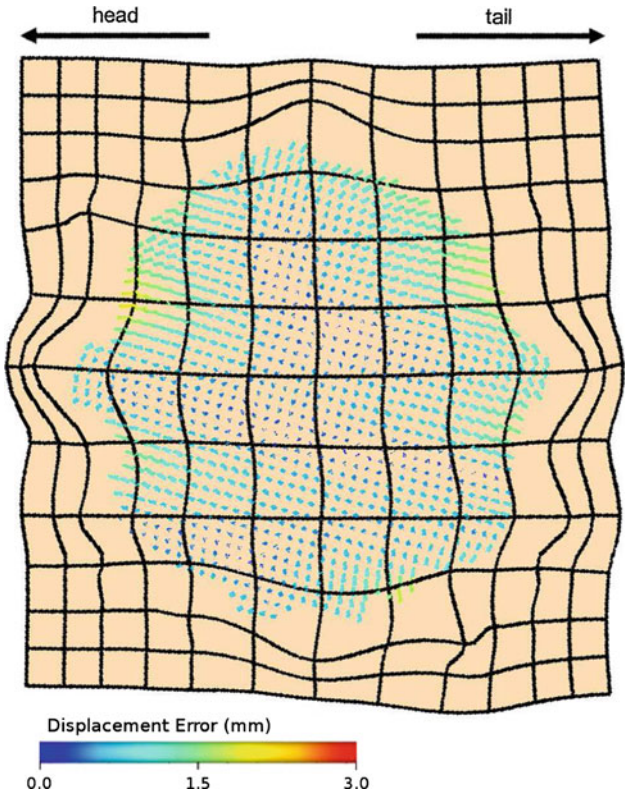

Fig. 8 The error distribution between experimentally measured and model-predicted material points for sample 7C5 at the optimum determined using *Strategy A*

in Table 4. An example of the distribution of displacement errors for sample 7C5 is shown in Fig. 8. Values of ground matrix stiffness ranged from 5 to 32 kPa. The mean orientations were similar across the three tissue samples, ranging between 167° and 178°, indicating that the fiber orientation mean deviated only 2°–13° from the torso midline. Collagen fiber stiffness varied greatly across the three samples, ranging from 48 to 366 MPa. The reported range of collagen fiber stiffness for tendons had also been large, ranging from 100 MPa to 1.2 GPa (van Brocklin and Ellis 1965; Wright and Rennels 1964). The mean displacement errors of the optimized models using *Strategy A* ranged between 0.64 and 0.90 mm. For *Strategy B*, the optimal values for K_m and μ_θ were similar to those identified using *Strategy A*. The mean undulation at the optimum ranged from 1.04 to 1.34 across all samples. The mean displacement errors of the models optimized using *Strategy B* ranged between 0.63 and 1.03 mm.

3.3 Identifiability of parameters

Of the 10 different sets of initial estimates used for *Strategy A*, only five sets converged to the global optimal solution for all tissue samples. By plotting the position of the optimum (denoted by the pink squares) in the 3D parameter space, together with the positions of the initial estimates (denoted by the colored spheres), only initial estimates with a mean orientation relatively close to the optimal mean orientation converged to the same optimum (denoted by

Table 4 Optimized parameters for each tissue sample using *Strategy A*

Strategy A	K_m (kPa)	μ_θ (rad)	K_c (MPa)	Mean ± SD displacement error (mm)	det($\mathbf{H}_0$)	cond($\mathbf{H}_0$)	det($\tilde{\mathbf{H}}_0$)
7C5	5.02	3.03	48.10	0.64 ± 0.38	5.76E+03	7.63E−04	0.45
9B4	6.98	3.11	156.30	0.90 ± 0.44	9.85E+01	3.00E−04	0.48
9C5	31.83	2.92	365.63	0.81 ± 0.48	3.33E−01	3.6E−05	0.37
Strategy B	K_m (kPa)	μ_θ (rad)	μ_x	Mean ± SD displacement error (mm)	det($\mathbf{H}_0$)	cond($\mathbf{H}_0$)	det($\tilde{\mathbf{H}}_0$)
7C5	4.99	3.03	1.34	0.63 ± 0.37	5.92E+04	7.68E−04	0.43
9B4	6.96	3.12	1.07	0.94 ± 0.42	1.53E+03	2.89E−04	0.83
9C5	30.98	2.95	1.04	1.07 ± 0.53	5.73E+02	3.48E−05	0.71

The M-optimality criterion (det($\mathbf{H}_0$)), condition number (cond($\mathbf{H}_0$)) and D-optimality criterion (det($\tilde{\mathbf{H}}_0$)s) at the optimum are also listed

the larger spheres). Figure 9a and c show that any initial estimates within 46° of the optimal mean orientation converged to the optimum, regardless of large variations in the initial estimates of K_m and K_c (Fig.9b). The initial estimates of μ_θ must be relatively close to the optimal values in order for the global minima to be found; thus, the identification problem was highly sensitive to μ_θ. This was confirmed for sample 7C5 by a relatively large component of the Hessian at optimum $\mathbf{H}_0(2, 2)$ associated with μ_θ, compared with the Hessian components associated with K_m, $\mathbf{H}_0(1, 1)$, and K_c, $\mathbf{H}_0(3, 3)$, as seen in Eq. 15. Similar observations were made for *Strategy B*, whereby the initial estimate for the mean orientation needed to be relatively close to the optimal mean orientation in order to achieve successful convergence.

$$\text{7C5: } \mathbf{H}_0 = \begin{bmatrix} K_m & \mu_\theta & K_c \\ 1.0 & -14.5 & -1.2 \\ -14.5 & 981.4 & 73.6 \\ -1.2 & 73.6 & 13.3 \end{bmatrix}, \qquad \tilde{\mathbf{H}}_0 = \begin{bmatrix} K_m & \mu_\theta & K_c \\ 1.00 & -0.47 & -0.34 \\ -0.47 & 1.00 & 0.64 \\ -0.34 & 0.64 & 1.00 \end{bmatrix} \tag{15}$$

3.4 Parameter correlation

The scaled Hessian at the optimum, $\tilde{\mathbf{H}}_0$, gives a measure of the correlation between the parameters. For *Strategy A*, the degree of interaction between fiber orientation mean (μ_θ) and collagen fiber stiffness (K_c) was consistently much greater than that between ground matrix stiffness (K_m) and μ_θ, or between K_m and K_c (Eq. 15). $\tilde{\mathbf{H}}_0$ showed an inverse relationship between K_m and μ_θ and between K_m and K_c. The overall interaction between all parameters identified was reflected by $\det(\tilde{\mathbf{H}}_0)$, whereby a value of 1 would indicate no interaction between the parameters. Values of $\det(\tilde{\mathbf{H}}_0)$ across the samples ranged between 0.37 and 0.48 (Table 4), indicating that the degree of interaction between the material parameters being identified was relatively large.

For *Strategy B*, the greatest interaction occurred between μ_θ and μ_x in an inverse manner. The interaction between K_m and μ_x was positive. The degree of parameter interaction was significantly smaller for samples 9B4 and 9C5, $\det(\tilde{\mathbf{H}}_0)$ ranging from 0.71 to 0.83, compared with the degree of interaction for the same samples using *Strategy A*. In contrast, the degree of parameter interaction with *Strategy B* for sample 7C5 was similar to that obtained using *Strategy A*.

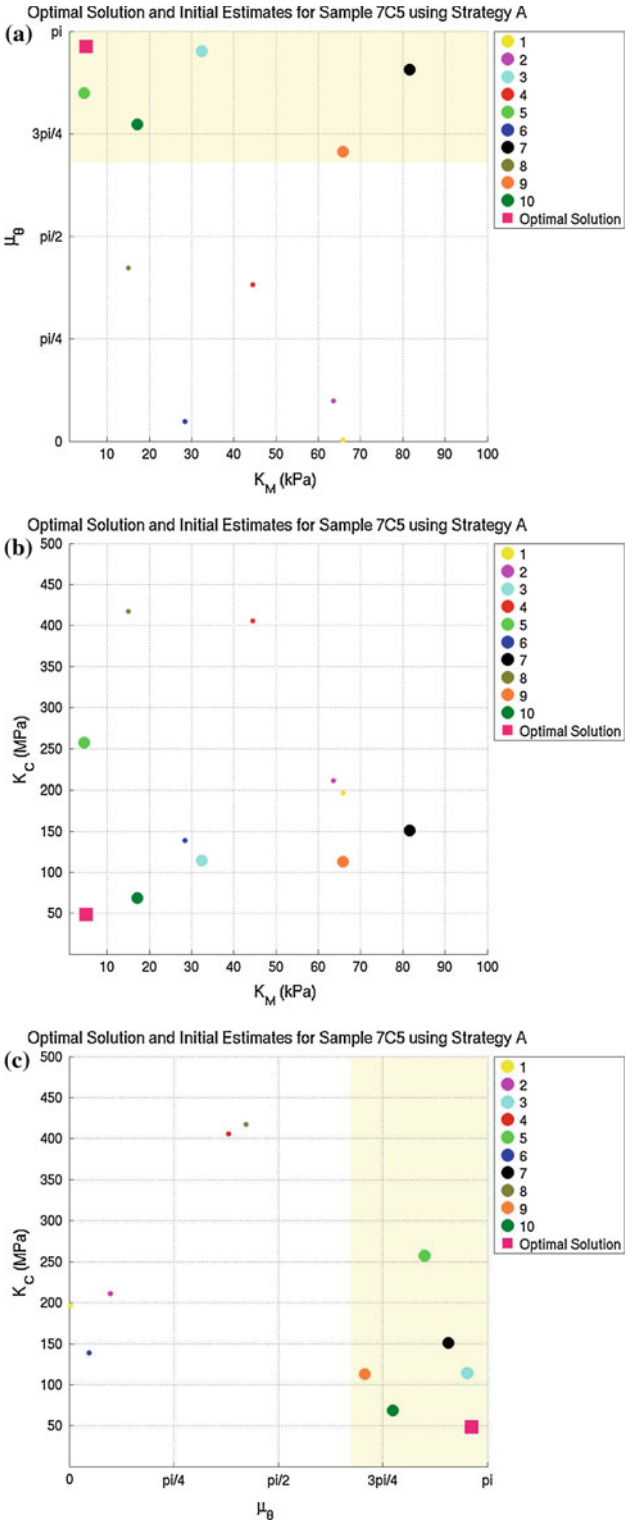

Fig. 9 The relationship between the positions of the optimum (shown as the *largest pink square*) and initial estimates within the 3D parameter space for sample 7C5, using *Strategy A*. Initial estimates that converged to the optimum are denoted by *larger dots* (i.e., Sets 3, 5, 7, 9 and 10), while initial estimates that did not reach the optimum are denoted by *smaller dots*. The region within the parameter space that converged to the same optimum are highlighted in *pale yellow* in (**a**) and (**c**)

4 Discussion

In this study, the results on the identification of material parameters of a structurally based constitutive relation based upon experimental data obtained from multi-axial tensile tests on porcine skin are presented. Three main components involved in the identification process were (1) measurements of displacement field data of material points from mechanical experiments; (2) FE modeling of the experiments; and (3) an iterative method of estimating the material parameters of the chosen constitutive relation to best match experimental displacements. Due to a large number of material parameters and their interactions in the chosen 2D constitutive relation, a subset of the ground matrix stiffness (K_m), fiber orientation mean (μ_θ) and collagen fiber stiffness (K_c) was identified for *Strategy A* and K_m, μ_θ and fiber undulation mean (μ_x) for *Strategy B*. Other parameters were fixed to values reported in the literature. The distribution and magnitude of mean displacement error were similar for both strategies and ranged from 0.63 to 1.07 mm across the samples. Limitations of the present modeling framework and the possible sources of modeling errors are listed below:

1. Analysis of the identifiability of the parameters reflected high sensitivity to fiber orientation mean. In this study, the fiber orientation mean for the tissue samples were not known. Although quantitative data on fiber orientation have been extracted from confocal images in a previous study, these analyzes have been performed on saggital, not parallel, sections. Furthermore, although the samples used in imaging and mechanical experiments were excised from similar body locations of the pig, it would be ideal to use the same specimen for both imaging and experimental purposes in any future work in order to eliminate any inter-specimen variations. Since *a priori* knowledge of fiber orientation mean is important to the success of parameter identification, quantitative image analysis of collagen orientation in the horizontal direction is of high priority in future work.
2. There is a large inter-specimen variability in collagenous tissues, such as the skin, making the determination of unique material parameters a challenging task. The high variability in the identified material parameters is likely to be due to this inter-specimen variability. The sources of variability may be attributed to differences in the strain history, internal tissue structure, age and experimental errors. Given that the inter-specimen variability in structural arrangement may be large, fixing structural parameters such as fiber orientation spread, undulation mean, undulation spread and fiber volume fraction of all the tissue samples to the same values (e.g., as reported in the literature) may potentially cause problems. This underscores the need for a richer set of structural information specific for the testing subject. All of the parameters that were fixed during the estimation procedure were structural parameters. The motivation for this was that structural parameters may be attainable through various types of imaging techniques. By collecting structural data from various body locations, the variability of structural components may be investigated with respect to body location. This would aid in determining the optimal size of a specimen to be used such that the assumption of homogeneous material properties is valid across the entire specimen. Alternatively, it may highlight the need for heterogeneous fields to describe spatially varying structural properties across the samples. In this study, the material properties were assumed to be homogeneous across the entire specimen.
3. One of the limitations of the current FE model was that elastin fibers were not included in the constitutive relation; hence, the mechanical response for smaller strains was assumed to be dominated by the ground matrix stiffness. Although the ground matrix contributes to the mechanical response at low strains, it does not provide any anisotropic effects. By omitting the elastin fiber network, the prediction of the mechanical response for low strains may not be appropriate. An extension to the current work would be to include an additional family of fibers into the constitutive framework to represent the structure and properties of elastin fibers. However, this omission is unlikely to affect the major outcomes of the present study.

The specific forms used to represent the structure (e.g., distributions to describe fiber orientation and undulations) and properties (e.g., fiber load–stretch relation) in the employed constitutive relation are not unique. The von Mises distribution to represent fiber orientation was chosen based upon its rotational symmetry and its ability to provide a good fit to the imaging data. However, other distributions may also be adequate. This is also the case for the choice of fiber undulation distribution. It may be advantageous to investigate other forms of distribution functions in future studies.

The use of two different constitutive parameter estimation strategies has shown that sets of optimal values using the present constitutive relation were not unique. Different sets of parameters resulted in similar magnitudes of error, indicating that the present sets of experimental data were not sufficient to uniquely characterize the parameters of the 2D constitutive relation. Further work could include performing non-equi-axial loading states, such as imposing a different extent of deformation along each of the 12 axes of the multiaxial rig. It was apparent that additional experimental data would be required in order for material parameters associated with the out-of-plane dimension to be reliably identified. In order to identify the parameters of a 3D biomechanical

model, experiments such as indentation and shear tests are likely to help (Flynn et al. 2010).

It was acknowledged that by using the preloaded geometry as the mechanical reference (i.e., stress-free) state in this study, the effects of pretension were neglected in the mechanical analyzes. Given that the magnitudes of the measured pretension forces were approximately 2–8% of the applied load, it was unlikely that the modeling results would be significantly affected by this omission from the mechanics analyzes. The choice of the preloaded geometry as the reference configuration resulted in a relatively good fit between experimental data and model results. However, the present model was not capable of accurately simulating the corresponding deformation when the unloaded geometry was used as the reference configuration. The changes in structural arrangement of different components and the interaction between them that occur during the early phases of deformation (i.e., from the unloaded to preloaded states) are likely to be complex. In contrast, deformation that occurs beyond the preloaded configuration corresponds to a steeper part of the stress–strain relationship, where mechanical response is better defined. It is therefore not surprising that the present model requires improvement before it is able to accurately predict the mechanical response using loads applied to the unloaded geometry. The omission of an elastin fiber network may be a significant factor in the mismatch between experimental and model predictions during the initial phases of the stress–strain response. Nevertheless, a biomechanical model of skin tissue is useful if it is capable of accurately predicting the mechanical response of skin within the physiological range (i.e., the preloaded configuration).

The experimental techniques and the structurally based biomechanical model developed in this study have been demonstrated to provide good fits to model parameters. The established framework is a valuable tool for future analyzes in order to better understand the nonlinear, anisotropic mechanical behavior of skin.

Acknowledgments The assistance from Dr C. Flynn in instrumentation and Mr P.B. Gamage in optimization are gratefully acknowledged. This publication is based on work supported in part by New Economy Research Fund (NERF) administered by the Foundation for Research, Science and Technology (FRST) and Award No KUK-C1-013-04, made by King Abdullah University of Science and Technology (KAUST). J.W.Y. Jor is supported by Tertiary Education Commission (TEC) Top Achiever's Scholarship and M.P. Nash is supported by a James Cook Fellowship administered by the Royal Society of New Zealand.

References

Barel AO, Courage W, Clarys P (1995) Suction method for measurement of skin mechanical properties: the cutometer. In: Handbook of noninvasive methods and the skin. CRC Press, London

Billiar K, Sacks M (2000) Biaxial mechanical properties of the native and glutarldehyde-treated aortic valve cusp: part II-A structural constitutive model. J Biomech Eng 122:327–335

Bradley CP, Pullan AJ, Hunter PJ (1997) Geometric modeling of the human torso using cubic Hermite elements. Ann Biomed Eng 25(1):96–111

Brown IA (1973) A scanning electron microscope study of the effects of uniaxial tension on human skin. Br J Dermatol 89(4):383–393

Craik JE, McNeil IRR (1965) Histological studies of stressed skin. In: Biomechanics and related bioengineering topics. Pergamon Press, Oxford, pp 159–164

Daly C (1966) The biomechanical characteristics of human skin. PhD thesis, University of Strathclyde, Scotland

Daly CH (1969) The role of elastin in the mechanical behavior of human skin. In: 8th Int. Conf. Med. Biol. Eng

Diridollou S, Patat F, Gens F, Vaillant L, Black D, Lagarde JM, Gall Y, Berson M (2000) In vivo model of the mechanical properties of the human skin under suction. Skin Res Technol 6(4):214–221

Finlay B (1969) Scanning electron microscopy of the human dermis under uni-axial strain. Biomed Eng 4(7):322–327

Flynn C, Taberner A, Nielsen PMF (2010) Mechanical characterisation of in vivo human skin using a 3D force-sensitive micro-robot and finite element analysis. Biomech Model Mechanobiol published online

Fung YC (1967) Elasticity of soft tissues in simple elongation. Am J Physiol 213(6):1532–1544

Harkness ML, Harkness RD (1959) Effect of enzymes on mechanical properties of tissues. Nature 183:1821–1822

Holzapfel G, Ogden R (2009) On planar biaxial tests for anisotropic nonlinearly elastic solids. A continuum mechanical framework. Math Mech Solids 14:474–489

Holzapfel G, Gasser T, Stadler M (2002) A structural model for the viscoelastic behavior of arterial walls: continuum formulation and finite element analysis. Eur J Mech A Solids 21:441–463

Horowitz A, Lanir Y, Yin FCP, Perl M, Sheinman I, Strumpf RK (1988) Structural three dimensional constitutive law for the passive myocardium. J Biomech Eng 110:200–207

Hurschler C, Loitz-Ramage B, Vanderby R (1997) A structurally based stress-stretch relationship for tendon and ligament. J Biomech Eng 119(4):392–399

Jor JWY, Nielsen PMF, Nash MP, Hunter PJ (2010) Modelling collagen fibre orientation in porcine skin based upon confocal laser scanning microscopy. Skin Res Technol (accepted)

Kvistedal YA, Nielsen PMF (2009) Estimating material parameters of human skin in vivo. Biomech Model Mechanobiol 8(1):1–8

Lanir Y (1979) A structural theory for the homogeneous biaxial stress-strain relationships in flat collagenous tissues. J Biomech 12(6):423–436

Lanir Y (1983) Constitutive equations for fibrous connective tissues. J Biomech 16(1):1–12

Lanir Y, Fung YC (1974) Two-dimensional mechanical properties of rabbit skin. I. Experimental system. J Biomech 7(1):29–34

Lokshin O, Lanir Y (2009) Micro and macro rheology of planar tissues. Biomaterials 30:3118–3127

Malcolm D (2000) Estimating the material properties of inhomogeneous elastic membranes. PhD thesis, University of Auckland

Manschot JFM (1985) The mechanical properties of human skin in vivo. PhD thesis, Nijmegen University, The Netherlands

Meijer R, Douven LFA, Oomens CWJ (1999) Characterisation of anisotropic and non-linear behaviour of human skin in vivo. Comput Methods Biomech Biomed Eng 2(1):13–27

Nathanson MH, Saidel GM (1985) Multiple-objective criteria for optimal experimental design: application to ferrokinetics. Am J Physiol 248:378–386

Nielsen PMF, Malcolm DTK, Hunter PJ, Charette PG (2002) Instrumentation and procedures for estimating the constitutive param-

eters of inhomogeneous elastic membranes. Biomech Model Mechanobiol 1(3):211–218

Pope FM, Martin GR, Lichtenstein JR, Penttinen R, Gerson B, Rowe DW, McKusick VA (1975) Patients with Ehlers-Danlos syndrome type IV lack type III collagen. Proc Natl Acad Sci USA 72(4):1314–1316

Reihsner R, Balogh B, Menzel EJ (1995) Two-dimensional elastic properties of human skin in terms of an incremental model at the in vivo configuration. Med Eng Phys 17(4):304–313

Rodrigues L (2001) EEMCO guidance to the in vivo assessment of tensile functional properties of the skin. Skin Pharmacol Appl Skin Physiol 14:52–67

Rose EH, Ksander GA, Vistnes LM (1976) Skin tension lines in the domestic pig. Plast Reconstr Surg 57(6):729–732

Sacks MS (2003) Incorporation of experimental derived fiber orientation into a structural constitutive model for planar collagenous tissues. J Biomech Eng 125(2):280–287

Tong P, Fung YC (1976) The stress-strain relationship for the skin. J Biomech 9(10):649–657

van Brocklin D, Ellis DG (1965) A study of the mechanical behavior of toe extensor tendons under applied stress. Arch Phys Med Rehabil 46:369–373

Viidik A (1980) In: Viidik A, Vuust J (eds) Biology of collagen, chap 17, pp 239–355

Wilkes GL, Brown IA, Wildnauer RH (1973) The biomechanical properties of skin. CRC Crit Rev Bioeng 1(4):453–495

Wright DG, Rennels DC (1964) A study of the elastic properties of planar fascia. J Bone Joint Surg 46:482–492